Flow characteristics and influence associated with inter-blade cavitation vortices at deep part load operations of a Francis turbine

IOP Conf. Series: Journal of Physics: Conf. Series **813** (2017) 012029 doi:10.1088/1742-6596/813/1/012029

Flow characteristics and influence associated with inter-blade cavitation vortices at deep part load operations of a Francis turbine

K. Yamamoto[1], A. Müller[1], A. Favrel[1], C. Landry[2], F. Avellan[1]

[1]EPFL Laboratory for Hydraulic Machines, Avenue de Cour 33bis, 1007 Lausanne, Switzerland

[2]Power Vision Engineering Sàrl, Chemin des Champs Courbes 1, 1024 Ecublens, Switzerland

E-mail: keita.yamamoto@epfl.ch

Abstract. At a deep part load operation, Francis turbines are subject to the formation of inter-blade cavitation vortices inside blade channels, however its characteristics are not fully understood yet. The present study aims to investigate the development of the inter-blade vortex as well as the flow characteristics associated with the vortex formation inside the blade channel, by using the unsteady RANS simulation. The velocity survey reveals the appearance of the back flow region in the vicinity of the hub near the trailing edge, which seems closely linked with the inter-blade vortex development. Furthermore, the local influence of the inter-blade vortex is evaluated by the specific energy loss calculated from the rothalpy in the blade channel. The comparison of the different operating conditions evidences the impact of the inter-blade vortex presence on the energy dissipation through the blade channel.

1. Introduction

It is well known that Francis turbines are subject to a various type of cavitation flows depending on its operating condition [1, 2]. In particular, the cavitation vortex rope developing in a draft tube at full load and part load operations prevents a stable operation of hydraulic machines, therefore several researches have been performed in different ways [3, 4, 5, 6]. Recently, Francis turbines are increasingly required to guarantee a secured operation especially at deep part load condition in order to enable a smooth integration of the renewable energy sources. In such operating condition, the cavitation vortex inside a blade-to-blade channel called inter-blade cavitation vortex is observed, however, its characteristics are insufficiently understood thus far.

In the framework of the HYPERBOLE research project, experiments and numerical simulations for the inter-blade cavitation vortex at deep part load operation have been conducted and reported, contributing to a better comprehension of its characteristics [7, 8, 9]. The present study aims to demonstrate the numerical investigations about the development and the characteristics of the inter-blade vortex by the unsteady RANS simulation. The simulated vortex structure is compared to the visualization results for the validation, then the structure of the flow inside the blade channel associated with the inter-blade vortex development is investigated. Furthermore, the specific energy loss is evaluated by the integration of the specific rothalpy through the blade channel, and the influence of the inter-blade vortex on the energy dissipation is investigated by comparison of different operating conditions.

2. Simulation setups

The numerical simulation is conducted by the unsteady RANS simulation using the commercial flow solver ANSYS CFX 17.1. The calculation domain used for the performed simulation is shown in Fig.1, which includes a spiral case, stay vanes, guide vanes, runner, and draft tube. The total number of the nodes are about 16 million nodes.

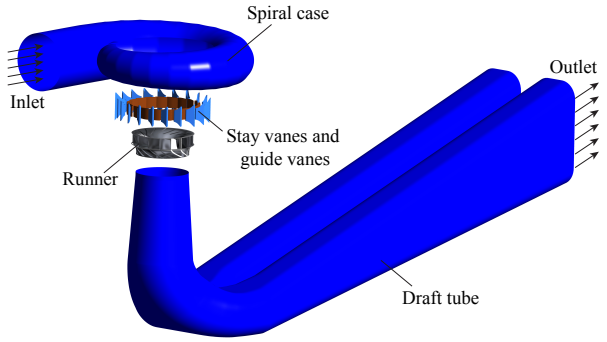

Figure 1. Calculation domain for unsteady RANS simulations

In the performed simulation, a two phase flow is treated as a homogeneous fluid assuming that the relative motion between phases can be neglected. Thus, the fluids in all the phases share a common flow field such as pressure and velocity. Cavitation is taken into account by solving the transport equation for the vapor volume fraction, based on the simplified Rayleigh-Plesset equation [10]. For a time step of the simulation, 0.0001 s corresponding to about 0.5 degree of the runner revolution is selected.

For a turbulence model, SST-SAS model is adopted. This model provides results similar to LES (Large Eddy Simulation), particularly in the unsteady flow region [11]. It has been shown that the model is used for various industrial applications with satisfactory results in recent years [12], including the simulation of the inter-blade cavitation vortex [9].

In the performed simulation, the following operating conditions (see Table 1) at the constant guide vane opening 5 degree are targeted for the comparison of the results. The n_{ED} value of OP2 is equivalent to the rated n_{ED} condition.

Table 1. Targeted operating conditions

OP	α	Runner rotation n	Specific energy E	n_{ED}	Q/Q_{BEP}	σ
1	5 (deg)	14.67 (Hz)	263 (J kg^{-1})	0.317 (-)	0.265 (-)	0.11 (-)
2	5 (deg)	13.33 (Hz)	263 (J kg^{-1})	0.288 (-)	0.270 (-)	0.11 (-)
3	5 (deg)	12.90 (Hz)	263 (J kg^{-1})	0.268 (-)	0.273 (-)	0.11 (-)

3. Simulation result

In Fig.2, the instantaneous view of the vortex structure and cavitation as well as the averaged vortex structure over four runner revolutions are shown. The vortex structure is detected by the non-dimensional Q-criterion which is calculated by the invariant of the velocity gradient tensor $\mathbf{L} = \nabla \mathbf{W}$, as in;

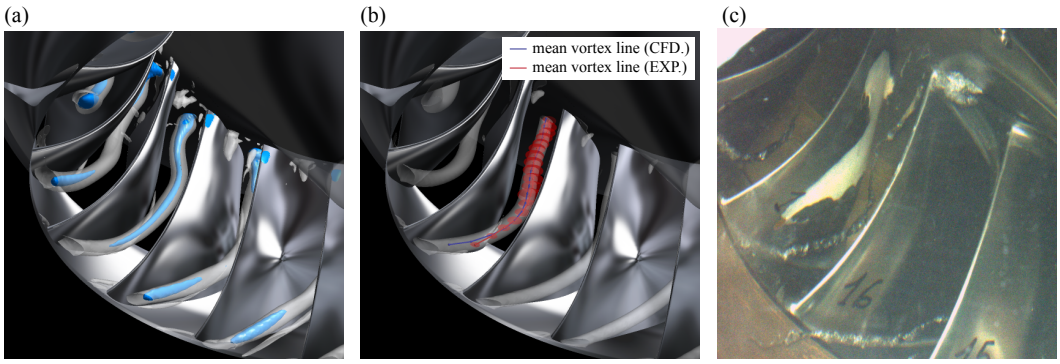

Figure 2. Instantaneous view of the simulated inter-blade vortex structure (white surface) and cavitation (blue surface, iso-surface of vapor volume fraction 10 %), averaged vortex structure together with the mean vortex lines (b) and the experimental visualization of the inter-blade cavitation vortex (c)

$$Q^* = \left(\frac{D_{ref}}{W_1}\right)^2 Q = \frac{1}{2}\left(\frac{D_{ref}}{W_1}\right)^2 [(tr(\mathbf{L}))^2 - tr(\mathbf{L}^2)] \tag{1}$$

where D_{ref} represents a reference diameter of the runner, W_1 a relative velocity at the runner inlet, and $tr(\mathbf{L})$ a first invariant of the velocity gradient tensor. In the presented case, the value of $Q^* = 3.0 \times 10^4$ is chosen to highlight the inter-blade vortex structure. In Fig.2(b), the comparison of the simulated location of the mean vortex center (see blue line in Fig.2(b)) with the vortex location of the experiment estimated based on the visualization (see red line in Fig.2(b)) is also presented. In the simulation result, the maximum value of the non-dimensional Q-criterion at each constant span-wise location is taken as the location of the vortex center. It can be confirmed that the both cavitation and inter-blade vortex structure are well captured by the performed simulation, moreover the simulated mean vortex location has a very good agreement with the experimental result.

In Fig.3, the distribution of the averaged non-dimensional meridional velocity C_m^* at the constant span-wise location in the vicinity of the hub ($s^* = 0.99$) as well as the meridional distribution of C_m^* at OP1 are shown. C_m^* is normalized by using the mean meridional velocity at each streamwise section and then averaged over four runner revolutions. At $s^* = 0.99$, it is shown that the high meridional velocity region appears at the inlet of the blade channel, whereas the velocity becomes remarkably low at the outlet of the runner. In particular, near the trailing edge on the suction side the flow is dominated by the back flow region. The development of the back flow region near the hub is also confirmed by the meridional contour of C_m^* (see Fig.3(b)). It demonstrates that the high velocity flow is consolidated in the vicinity of the shroud especially at the outlet of the blade, on the other hand the flow near the hub is dominated by the back flow region close to the hub. The development of the back flow region on the hub starts at the streamwise location $m^* = 0.60$, which corresponds to the inception of the inter-blade vortex. This evidently confirms that the occurrence of the inter-blade vortex development is closely relevant to the formation of the back-flow region in the vicinity of the hub near the exit of the blade channel. It should be noted that the formation of the back flow region as well as the strength of the inter-blade vortex are drastically reduced at OP2 and OP3.

4. Local influence of the inter-blade vortex

In the present study, the local influence of the inter-blade vortex is evaluated by the specific rothalpy which is used for the quantitative evaluation of the specific energy loss inside the

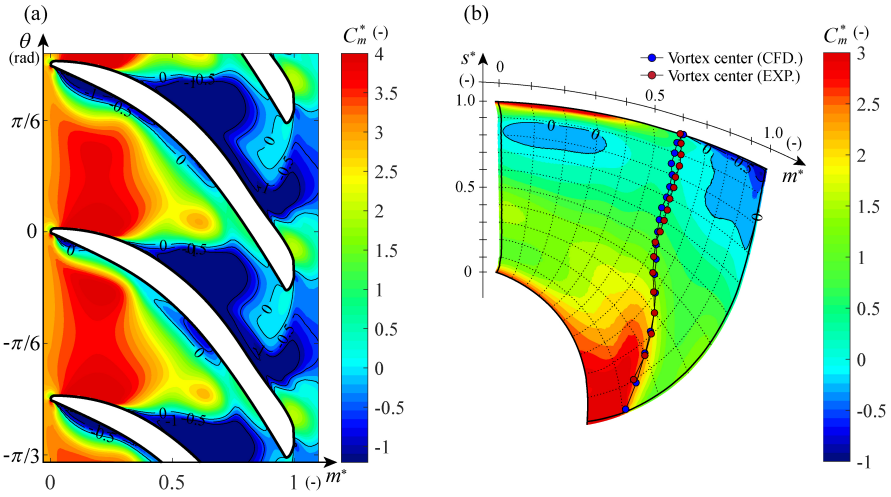

Figure 3. Meridional velocity contour at $s^* = 0.99$ (a) ($m^* = 0$ at the leading edge and 1 at the trailing edge) and at the meridional plane together with the projected inter-blade vortex location(b) at OP1

runner. The variation of an energy flux defined by the specific rothalpy I through a control volume rotating with the runner is expressed as;

$$\Delta F_I = \int_{\partial V} \left(\frac{p}{\rho} + \frac{1}{2}\vec{W}^2 - \frac{1}{2}(r\omega)^2 + gz \right) \rho \vec{W} \cdot \vec{n} dA \equiv \int_{\partial V} I \, \vec{W} \cdot \vec{n} dA \tag{2}$$

where p represents the static pressure, r the radius, ω the angular rotational frequency, and z the elevation. In the previous study, it was proven that the energy flux ΔF_I is conserved under specific conditions [13], however in the real flow, ΔF_I is dissipated due to the viscosity and the unsteadiness of the flow. By setting the boundaries of the control volume on a plane of a constant streamwise location m^* and the blade channel wall boundaries, the specific energy loss E_r from the blade inlet to a given streamwise location m^* can be calculated as;

$$\begin{aligned} E_{r_{1 \div m^*}} &= \frac{1}{\rho Q} \left(\int_A I \, \rho \vec{W} \cdot \vec{n} dA \Big|_{m^*} - \int_A I \, \rho \vec{W} \cdot \vec{n} dA \Big|_{m^*=0} \right) \\ &= \frac{1}{\rho Q} \left(\int_{z_{sh}}^{z_{hb}} \int_{\theta_s}^{\theta_p} \rho C_m I r sin\gamma \, d\theta dz \Big|_{m^*} - \int_{z_{sh}}^{z_{hb}} \int_{\theta_s}^{\theta_p} \rho C_m I r sin\gamma \, d\theta dz \Big|_{m^*=0} \right) \end{aligned} \tag{3}$$

where z_{hb} and z_{sh} are the axial position of the hub and shroud at a given streamwise location, θ_s and θ_p are the angular position of the suction side and the pressure side of the blade, γ the deflection angle between the span-wise plane and the z-axis. The specific energy dissipation rate is then calculated using the specific energy loss E_r, as in;

$$e = 1 - \frac{E_{r_{1 \div m^*}}}{E_{blade}} \tag{4}$$

where E_{blade} is the specific energy of the evaluated blade channel. In Fig.4, the evolutions of the specific energy dissipation rate e as well as the derivative of e over the streamwise location m^* for three different operating conditions are shown. It demonstrates that the energy dissipation rate is almost constantly decreased near the inlet, however the slope of the decrease is clearly modified around $m^* = 0.55$ which almost corresponds to the region where the inter-blade vortex

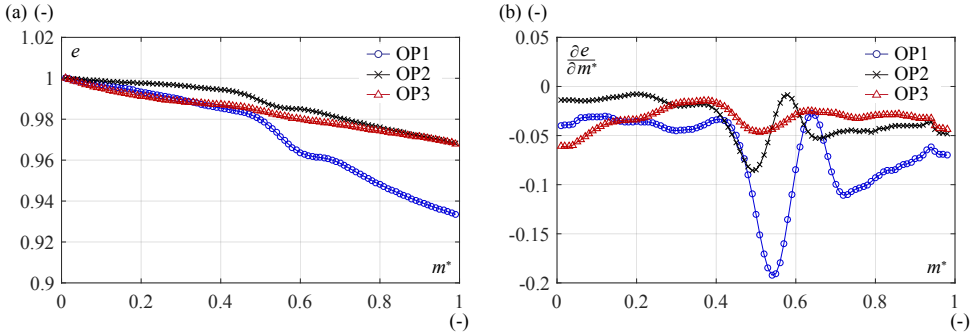

Figure 4. Evolution of the specific energy dissipation rate (a) and the gradient of the energy dissipation rate over the streamwise location (b) for three operating conditions

starts to develop. This significant change is most obvious at OP1, then it is reduced at OP2 and OP3 in accordance with the reduction of the inter-blade vortex intensity. The derivative of e is also significantly amplified at OP1, which evidently shows that the presence of the inter-blade vortex induces the energy dissipation through the blade channel.

5. Conclusion

It is shown that the inter-blade cavitation vortex is successfully captured by the performed unsteady RANS simulation, which is validated by the visualization results. The meridional velocity survey demonstrates the highly non-uniform flow distribution inside the blade channel especially in the vicinity of the hub. Moreover, it evidences the formation of the back flow region around the hub close to the trailing edge, which plays a significant role for the inter-blade vortex development. Furthermore, the negative impact of the inter-blade vortex on the specific energy is confirmed by the energy dissipation evaluated by the specific rothalpy through the blade channel.

Acknowledgments

The results presented in the paper is part of the HYPERBOLE research project, granted by the European Commission (ERC/FP7-ENERGY-2013-1-Grant 608532).

References

[1] Avellan F 2004 *Proceedings of the 6th International Conference on Hydraulic Machinery and Hydrodynamics, Timisoara, Romania*
[2] Escaler X, Egusquiza E, Farhat M, Avellan F and Coussirat M 2006 *Mechanical Systems and Signal Processing* **20** 983–1007
[3] Favrel A, Müller A, Landry C, Yamamoto K and Avellan F 2015 *Experiments in Fluids* **56** 1–15
[4] Favrel A, Mller A, Landry C, Yamamoto K and Avellan F 2016 *Experiments in Fluids* **57**
[5] Müller A, Dreyer M, Andreini N and Avellan F 2013 *Experiments in Fluids* **54**
[6] Landry C, Favrel A, Mller A, Nicolet C and Avellan F 2016 *Journal of Hydraulic Research* **54** 185–196
[7] Yamamoto K, Müller A, Favrel A, Landry C and Avellan F 2013 *IOP Conference Series: Earth and Environmental Science* **22**
[8] Yamamoto K, Müller A, Favrel A, Landry C and Avellan F 2015 *Proceedings of the 6th IAHR International Meeting of the Workgroup on Cavitation and Dynamic Problems in Hydraulic Machinery and Systems, Ljubljana, Slovenia*
[9] Wack J and Riedelbauch S 2015 *Journal of Physics: Conference Series* **656**
[10] Zwart P, Gerber A G and Belamri T 2004
[11] Egorov Y and Menter F 2008 *Notes on Numerical Fluid Mechanics and Multidisciplinary Design* **97** 261–270
[12] Menter F and Egorov Y 2010 *Flow, Turbulence and Combustion* **85** 113–138
[13] Lyman F 1993 *Journal of Turbomachinery* **115** 520–526